JOURNAL OF MATERIALS SCIENCE 8 (1973) 1699–1705

Strength-probability-time (SPT) relationships in ceramics

R. W. DAVIDGE, J. R. McLAREN, G. TAPPIN
Materials Development Division,
AERE, Harwell, Berks, UK

The concept of the SPT diagram for ceramics is introduced as an essential aid to the design engineer when using engineering ceramics. For given conditions of stress state and distribution, environment, temperature and component size, the diagram enables estimates of a safe working stress to be made for specific component lifetimes and survival probabilities. The theory underlying the SPT diagram is reviewed. This involves the merging of the concepts of statistical variations in strength, with sub-critical crack growth which leads to delayed fracture. It is shown how the SPT diagram can be generated by simple measurements of the strain rate dependence of fracture strength. Data for the delayed fracture of alumina are used to demonstrate the reliability of SPT diagram.

1. Introduction

As the widespread use of ceramics as engineering components becomes increasingly likely, it is clear that the materials scientist is to some extent failing in his duty to supply the design engineer with mechanical property data in the most appropriate form. This leads to *ad hoc* and iterative design procedures, the efficiency of which could be greatly enhanced by the improved presentation of data. By far the most common strength test is the measurement of modulus of rupture: a bar is broken in three- or four-point bending and the strength is quoted as the maximum tensile stress sustained by the specimen. This is a simple test to perform and is very useful for a rapid evaluation of materials on a comparative basis. Furthermore, basic theory has been developed to a stage where there is an excellent fundamental understanding of strength in terms of microstructural parameters [1-3].

However, this information is of limited use to the design engineer. Additionally, information is required on the statistical variation in strength or probability of failure at a particular stress level; effects of static and dynamic fatigue; effects of environment and temperature; and effects of multiaxial stresses. All of these are being actively studied at present. It is the purpose of this paper to describe how information on the first two areas can be presented on a strength-probability-time (SPT) diagram using information derived from simple experimental techniques In this way, a component operating under known conditions of stress state, environment and temperature can be designed with regard to component lifetime and acceptable probability of failure. Considerations of statistical variations of strength, and stress intensity factor/crack velocity data are required and these are discussed below.

2. Statistical variations in strength

The strength (σ_f) of ceramics is controlled generally by the stress to propagate small microstructural flaws, which are invariably present, according to a modified Griffith equation,

$$\sigma_f = \frac{1}{Y}\left(\frac{2E\gamma_i}{C}\right)^{\frac{1}{2}} \quad (1)$$

where Y is a geometrical constant, E Young's modulus, γ_i an effective surface energy, and C a flaw size. Because a given ceramic will have a range of flaw sizes there will be a corresponding variation in strength. In principle, one could rationalize this in terms of the variables in Equation 1 but this has yet to be achieved. Fortunately, an empirical statistical analysis is available and that of most widespread (but not

universal) applicability is the weakest link model due to Weibull [4, 5].

$$P = \exp\left[- D \left(\frac{\sigma_f - \sigma_u}{\sigma_0} \right)^m \right], \quad (2)$$

where P is the survival probability, D the stressed volume, σ_u the zero probability stress, σ_0 a normalizing constant, and m the Weibull modulus. Thus

$$\ln \ln \frac{1}{P} = m \ln (\sigma_f - \sigma_u) - m \ln \sigma_0 + \ln D. \quad (3)$$

Intuitively, $\sigma_u = 0$ and this is often found experimentally. A plot of ln ln $1/P$ versus ln σ_f thus gives the Weibull modulus m. (Should this treatment not yield a straight line relationship, then other statistical functions, such as normal or log normal strength variations, may be appropriate [6].) As an example of a material showing a Weibull distribution of strength, Fig. 1 gives

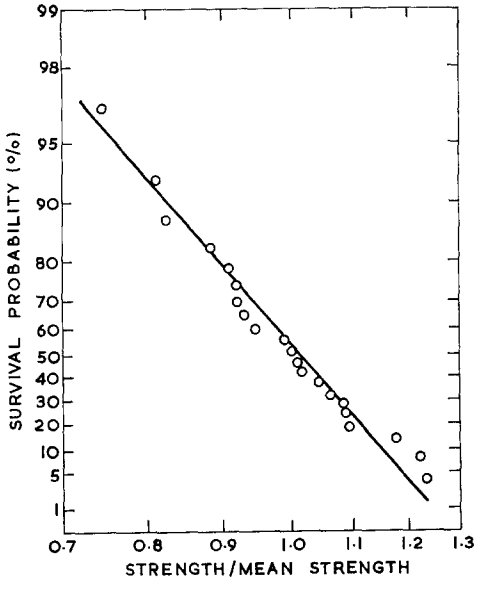

Figure 1 A Weibull distribution of strength for tensile specimens of Refel SiC [7].

data for Refel SiC tested under tension [7]. A reasonable straight line relationship is found, giving a Weibull modulus m of 10 which is typical for good quality ceramics. The above discussion relates only to short term strength. The effect of time under stress is considered next.

3. Time-dependent failure

A wide range of materials, including ceramics, exhibits the phenomenon of delayed fracture or static fatigue [8-12]. Under the application of stress less than that to induce short term failure, there is a regime where sub-critical crack growth can occur leading to failure in finite times. The effect is believed to be due to a stress-dependent chemical interaction between the material and its environment. Water, for example, has a pronounced deleterious effect on the strength of glass and alumina. Recent theoretical and experimental work in this area has demonstrated that time-dependent failure characteristics can be understood and predicted in a quantitative way by consideration of crack velocity/stress intensity factor data.

Rearranging Equation 1 and defining a critical stress intensity factor K_{Ic} as $(2E\gamma_i)^{\frac{1}{2}}$

$$K_{Ic} = Y \sigma_f C_c^{\frac{1}{2}} \quad (4)$$

where the subscript c refers to the critical condition. New test methods have been evolved whereby the crack velocity (V) in a specimen can be recorded simply in terms of K_I; a convenient method [14, 15] is the double torsion test. The important feature is that the strain energy release rate, at constant force, G ($=2\gamma$), is independent of crack length. Thus, unlike most other tests, there is no tendency for the crack to accelerate under a constant critical load and produce catastrophic failure.

Data for alumina tested under ambient laboratory conditions are given in Fig. 2 [13]. There are two main regions:

$$\text{region I}, \quad V = \alpha_1 K_I^n \quad (5a)$$

$$\text{region II}, \quad V = \alpha_2 \quad (5b)$$

where the α's are constants. In region I, the rate of chemical reaction at the crack tip controls crack growth, whilst in region II diffusion of the corrosive species to the crack tip controls growth [8]. A region III is sometimes present but the fundamental rate controlling mechanisms are not fully understood at present. Also included in the diagram is the value of K_{Ic}

The K-V diagram can thus be obtained by straightforward experimental techniques and the data are understood in terms of fundamental mechanisms. The significance of the diagram in terms of crack growth is as follows. A particular specimen has an initial flaw size C_i. Application of a stress σ produces a stress intensity factor K_I ($= Y \sigma C^{\frac{1}{2}}$) corresponding to a crack velocity V. In a standard strength evaluation test, say a bend test, C thus increases to give a higher K_I

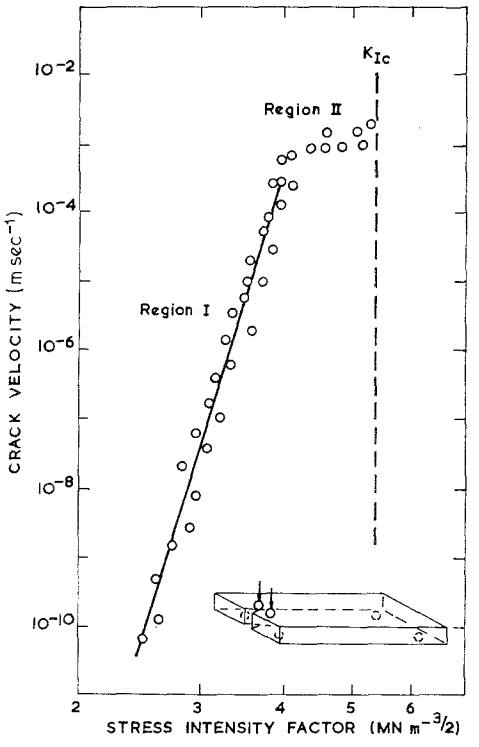

Figure 2 K-V diagram obtained from double torsion specimens for Al_2O_3 under ambient laboratory conditions [13].

and, in region I, a rapidly accelerating crack growth. When K_I reaches a particular value, (which may be less than K_{Ic}, depending on the environment) owing to increases in C, σ or both, catastrophic failure occurs.

Under constant σ, of interest in a delayed fracture test, the time to failure, τ, is given by

$$\tau = \int_{Ci}^{C_{Ic}} \frac{dC}{V} \tag{6}$$

The time for $C > C_{Ic}$ is negligible. From Equation 4,

$$dC = \frac{2K_I}{\sigma^2 Y^2} dK_I, \tag{7}$$

and substitution into Equation 6 gives

$$\tau = \frac{2}{\sigma^2 Y^2} \int_{KIi}^{K_{Ic}} \frac{K_I}{V} dK_I. \tag{8}$$

Recalling Equation 5, and defining K_I^* as the value separating regions I and II,

$$\tau = \frac{2}{\sigma^2 Y^2} \left\{ \frac{1}{a_1} \int_{KIi}^{K_I^*} K_I^{(1-n)} dK_I + \frac{1}{a_2} \int_{K_I^*}^{K_{Ic}} K_I dK_I \right\}. \tag{9}$$

A third term corresponding to region III may be added but this is generally negligible. Depending on the environment the second term (region II) is often negligible.

In a number of ceramics tested under ambient conditions, the time to failure is controlled solely by the behaviour in region I of the K-V diagram and Equation 9 reduces to

$$\tau = \frac{2}{\sigma^2 Y^2 a_1 (n-2)} \left\{ K_{Ii}^{2-n} - K_I^{*2-n} \right\}, \tag{10}$$

and furthermore, because n is large (typically > 10), $K_{Ii}^{2-n} \gg K_I^{*2-n}$, and

$$\tau = \frac{2 K_{Ii}^{2-n}}{\sigma^2 Y^2 a_1 (n-2)}. \tag{11}$$

4. The SPT diagram

The statistical effects can now be combined with the time-dependent failure analysis to give the SPT diagram. A given batch of N specimens will have a range of initial flaw sizes C_1 to C_N. For a particular specimen with a flaw size C_j (unknown until tested) the time to failure, combining Equations 4 and 11, is

$$\tau = \frac{2 Y^{2-n} \sigma^{2-n} C_j^{(2-n)/2}}{\sigma^2 Y^2 a_1 (n-2)} = \frac{a_3 C_j^{(2-n)/2}}{\sigma^n}. \tag{12}$$

Thus for specimens with the same intitial flaw size, and the same probability of instant failure,

$$\tau \sigma^n = a_4. \tag{13}$$

A family of lines can thus be constructed on a Weibull strength/probability-of-survival graph corresponding to increasing failure times (Fig.3). Note that these are equi-spaced for equal logarithmic increases in failure time. An individual specimen stressed at σ_j and failing in time τ_j is, therefore, equivalent to a specimen failing at stress σ_0 in a reference time τ_0, as indicated in Fig. 3, according to

$$\left(\frac{\sigma_0}{\sigma_j}\right)^n = \frac{\tau_j}{\tau_0}. \tag{14}$$

5. Delayed fracture tests and the relation to constant strain-rate tests

For any stress/failure time combination it is

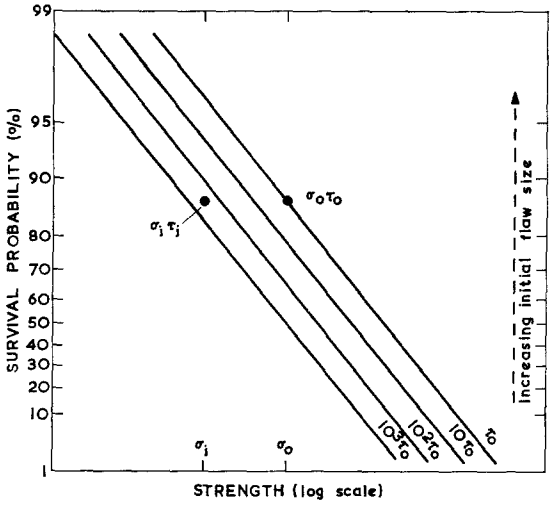

Figure 3 Method of relating delayed fracture data to "instantaneous" strength values with SPT diagram. Specimen failing at stress σ_j in time τ_j would have failed at stress σ_0 in time τ_0.

thus possible to normalize the data to time τ_0. It follows, therefore, that if a set of stress/failure time data is generated for a sample population of specimens, and normalized to time τ_0, then the statistical distribution of these normalized strengths should be related to that found from direct measurement of the strength at a particular strain-rate of a second sample population.

A convenient method of generating the delayed fracture data is to stress specimens from a sample at low stresses corresponding to a very high probability of survival. The stress is maintained for up to a fixed convenient time. Those specimens surviving are then stressed at a higher level, and the process repeated until all have failed. This assumes that the stressing at lower levels does not affect significantly the time to the failure at the ultimate failure stress. This, however, is essentially the same assumption used in deriving Equation 11.

To relate the results obtained under conditions of constant strain (or stress) rate to the delayed fracture data, it is necessary to calculate the characteristic time τ_c corresponding to the lifetime of a specimen stressed solely at σ_f, the strength under constant strain-rate. If the failure time under constant strain-rate is τ^*, then $\tau_c \ll \tau^*$ because in the constant strain-rate test there is little sub-critical crack growth until σ is close to σ_f.

For a given specimen $\tau\sigma^n = \alpha_4$ under constant stress. Under increasing stress the fraction of the specimen lifetime dt/τ spent at stress σ is $dt\,\sigma^n/\alpha_4$. Thus integrating over time,

$$1 = \int_0^{\tau^*} \frac{\sigma^n}{\alpha_4}\,dt\,. \tag{15}$$

Substituting $\alpha_4 = \tau_c\sigma_f{}^n$, and $dt = \tau^*\,d\sigma/\sigma_f$ gives

$$1 = \int_0^{\sigma_f} \frac{\tau^*}{\tau_c}\frac{\sigma^n}{\sigma_f{}^{n+1}}\,d\sigma. \tag{16}$$

Thus,

$$\tau_c = \frac{\tau^*}{n+1}\,. \tag{17}$$

From Equation 17 the ratio of the characteristic times for tests under two strain-rates $\dot\epsilon_1$, $\dot\epsilon_2$ will equal the ratio of the times to failure (τ_1, τ_2) at the two strain-rates. Thus for a given probability of failure (same initial flaw size)

$$\sigma_{1,2} = E\dot\epsilon_{1,2}\,\tau_{1,2} \tag{18}$$

where $\sigma_{1,2}$ are the strengths for a particular failure probability. Therefore, from Equation 13,

$$\frac{\sigma_1{}^{n+1}}{E\dot\epsilon_1} = \frac{\sigma_2{}^{n+1}}{E\dot\epsilon_2} \tag{19}$$

or

$$\left(\frac{\sigma_1}{\sigma_2}\right)^{n+1} = \frac{\dot\epsilon_1}{\dot\epsilon_2}\,. \tag{20}$$

Measurement of strength as a function of strain rate thus provides a simple way to estimate n A more rigorous mathematical approach leads to similar expressions to the above [16, 17].

6. Experimental and results

A 95% alumina was used, similar to that studied previously [18-20]. Specimens were machined to 25 × 3 × 2.5 mm, and tested in three-point bending (20 mm span) under ambient laboratory conditions. A batch of twenty-six specimens was broken under a strain-rate of 1.8×10^{-5} sec^{-1} ($\dot\epsilon_2$). Results are plotted in Fig. 4 which give a good fit to the Weibull distribution with a Weibull modulus of 13.2 and a mean strength of 361 MN m^{-2}. The time to failure at this mean stress is 60 sec. Two further batches each of nine specimens were broken under strain-rates of 1.8×10^{-6} and 1.8×10^{-4} sec^{-1} ($\dot\epsilon_1$ $\dot\epsilon_3$) (Fig. 4). Mean strengths are, respectively, 322 and 395 MN m^{-2}. In these cases the slope of the Weibull line has been drawn parallel to the $\dot\epsilon_2$ data even though the best fit lines would be slightly different. This is because of the greater confidence

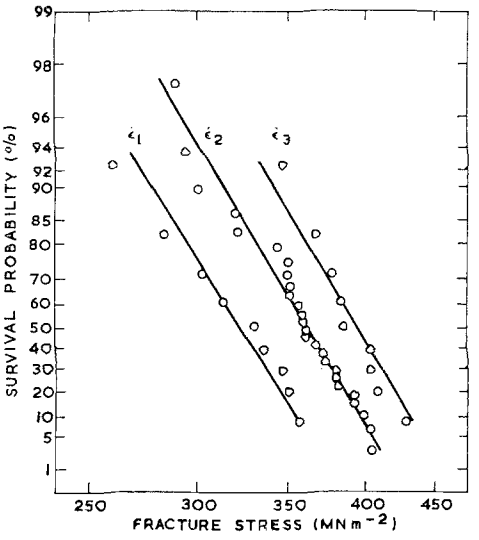

Figure 4 Statistical variation in the strength of Al_2O_3 tested at three strain-rates.

in the $\dot{\epsilon}_2$ data, taken from a larger sample. The mean ratio of strengths for an order of magnitude change in strain-rate is 1.108, and use of Equation 20 gives $n = 21.5$.

A batch of twenty-five similar specimens was broken under delayed fracture conditions, also in three-point bending and 20 mm span, under constant stresses in the range 260 to 310 MN m^{-2}. In cases where the specimen did not break in a conveniently short time (overnight or a week-end) the stress was increased by 10 MN m^{-2}, several times if necessary. Results are detailed in Table I. Where a specimen has been stressed at several levels the failure time is taken as that solely at the maximum stress.

The relevant part of the K-V diagram was obtained from double torsion specimens 75 × 25 × 3 mm with a 0.5 mm deep guide groove. Data over the crack velocity range 10^{-3} to 10^{-7} m sec^{-1} give the expected $K \alpha V^n$ relationship in region I with $n = 30$ to 60. The bendover into region II occurs at $V \sim 10^{-3}$ m sec^{-1}. The equivalent γ_i value for the rapid propagation of the crack is 45 J m^{-2}.

7. The SPT diagram for alumina

The values of n obtained from double torsion specimens are considerably greater than those from the strain-rate data. The former relate to the propagation of a large preformed crack and the latter to the initial stages in the propagation of the small inherent flaws. These flaws are typically 50 μm deep and may grow 10 to 20 μm during the sub-critical range. Clearly the morphologies of the inherent flaw and the preformed crack are not identical and it cannot be assumed that data from macroscopic cracks are relevant to the propagation of microscopic cracks. For MgO, γ_i shows a marked dependence on crack length and γ_i increases by a factor of four as the crack size increases from one to ten grains [21]. There is no evidence for such marked behaviour in other ceramics and the "macroscopic" γ_i values lead to credible strength estimates with the flaw size related to grain size or pore size [1-3]. However, this argument does not necessarily apply to the current discrepancy

TABLE I Delayed fracture data

Specimen number	Stress (MN m^{-2})	Failure time (sec)	σ_e (1 sec) (MN m^{-2})	Rank
1	305	5	327	4
2	300	9000	457	23
3	305	365	404	16
4	305	185	389	12
5	292	247	377	11
6	295	60	357	7
7	286	1080	395	14
8	273	10	304	1
9	275	2160	390	13
10	280	4680	414	20
11	257	2340	369	9
12	274	45	327	3
13	274	68	333	5
14	275	69	334	6
15	270	> 9360		
	280	30	326	2
16	270	> 9000		
	280	> 5820		
	290	6480	435	22
17	270	5040	398	15
18	270	1010	370	10
19	270	580	363	8
20	270	> 60660		
	280	> 19260		
	290	> 2880		
	300	> 3600		
	310	48890	511	25
21	282	2845	407	17
22	270	16990	423	21
23	270	7850	408	18
24	270	> 71820		
	280	> 3060		
	290	> 3250		
	300	17675	472	24
25	270	> 10150		
	280	> 6030		
	290	2450	413	19

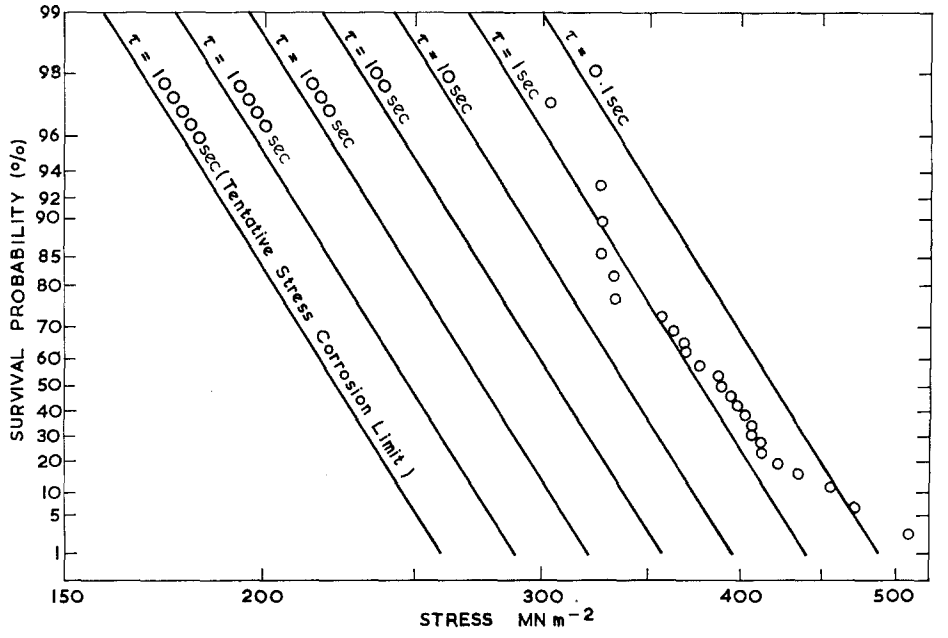

Figure 5 The SPT diagram for Al_2O_3. Superimposed are the delayed fracture data normalized to a failure time $\tau = 1$ sec.

and it must be concluded that the surface energy requirements for the sub-critical propagation of the crack are significantly less than those calculated from the macroscopic data. For these reasons, therefore, and because identical specimens are used for the strain-rate and delayed fracture tests, the value of n from the strain-rate data is used to generate the SPT diagram.

The SPT diagram is given in Fig. 5. The "anchor" point is taken from the $\dot{\epsilon}_2$ data at 361 MN m^{-2}, 50% survival probability, and characteristic failure time 2.67 sec (calculated from Equation 17). The characteristic failure times at the 1 and 99% survival probabilities are 3.10 and 1.95 sec. Thus the slopes of the lines on the SPT plot are slightly less than the Weibull slope. The line spacings for decade steps in time correspond to stress ratios of 1.11, from Equation 13.

As a check on the applicability of the above analyses, the delayed fracture data have been used to estimate (from Equation 14) the equivalent failure stresses for each specimen for a standard failure time of 1 sec; these are indicated in Table I and have been ranked in increasing order of stress. These data when transposed on the SPT diagram should thus fall on the 1 sec line and Fig. 5 shows that the agreement is remarkably good. Ignoring the five points corresponding to the strongest specimens, which will be discussed below, the remaining twenty points fall very close to the 1 sec line. The best fit line through these points would lie parallel to the 1 sec line and displaced to higher stress by a small factor, $< 3\%$.

The points ranked 21 to 25 correspond to those specimens with failure times > 6000 sec, and only one other specimen, ranked 18, falls into this range. These data are equivalent to mean crack velocities $\sim 10^{-9}$ m sec^{-1} which are well outside the velocity range examined in this study and close to the limit of published data [13] for Al_2O_3. In glass [16], a stress corrosion limit has been detected equivalent to a crack velocity of 3×10^{-10} m sec^{-1}. It is considered, therefore, that the deviation from expected behaviour of the data for specimens with velocities in this range may be indicative of a stress corrosion limit in Al_2O_3. It follows that the observed failure times for these specimens and the calculated stresses for 1 sec failure may be larger than predicted by the basic theory. The important consequence is that the (say) $\tau = 100000$ sec line of the SPT diagram may be considered as a tentative stress corrosion limit. Experimental verification of this would, however, be tedious because of the very long experimental times involved.

The use of the SPT diagram for engineering design purposes is straightforward. Assuming that the diagram is relevant to a specific application with regard to stress state and distribution, environment, temperature and component size, then from the required component lifetime and survival probability a safe working stress can be estimated. For example, a component lifetime of 100 000 sec with a survival probability of 99% would require the working stress to be < 160 MN m^{-2}. Were this value to prove unacceptably low, then either re-design of the component to reduce the maximum stress or some form of proof test to remove the weaker components would be appropriate. It must be emphasized that the SPT diagram is valid only for the conditions under which the specimens are tested. For example, strong variations with temperature are expected, particularly in those ranges where limited plastic flow processes can assist crack growth.

References

1. R. W. DAVIDGE and A. G. EVANS, *Mater Sci. Eng.* **6** (1970) 281.
2. R. W. DAVIDGE, *Proc. Brit. Ceram. Soc.* **20** (1972) 364.
3. *Idem, Sci. Ceram.* **6** (1973) paper IX.
4. W. WEIBULL, *Ing, Vetenskaps. Akad. Handl.* **155** (1939) 5.
5. *Idem, J. Appl. Mech.* **18** (1951) 293.
6. A. G. EVANS, C. PADGETT and R. W. DAVIDGE, *J. Amer. Ceram. Soc.* **56** (1973) 36.
7. P. KENNEDY, J. V. SHENNAN, P. M. BRAIDEN, J. R. MCLAREN and R. W. DAVIDGE, *Proc. Brit. Ceram. Soc.* **22** (1973) in press.
8. S. M. WIEDERHORN, *J. Amer. Ceram. Soc.* **50** (1967) 407.
9. *Idem, Internat. J. Frac. Mech.* **4** (1968) 171.
10. *Idem, J. Amer. Ceram. Soc.* **52** (1969) 485.
11. S. M. WEIDERHORN and L. H. BOLZ, *ibid* **53** (1970) 543.
12. J. C. V. RUMSEY and A. L. ROBERTS, *Proc. Brit. Ceram. Soc.* 7 (1967) 233.
13. A. G. EVANS, *J. Mater. Sci.* 7 (1972) 1137.
14. J. A. KIES and A. B. J. CLARK, in "Fracture, 1969" ed. P. L. Pratt (Chapman and Hall, London, 1969) p. 483.
15. H. R. MCKINNEY and H. L. SMITH, *Bull. Amer. Ceram. Soc.* **50** (1971) 784.
16. A. G. EVANS and S. M. WIEDERHORN, *Internat. J. Frac. Mech.* in press.
17. A. G. EVANS, *ibid*, in press.
18. R. W. DAVIDGE and G. TAPPIN, *J. Mater. Sci.* **3** (1968) 165.
19. *Idem, Proc. Brit. Ceram. Soc.* **15** (1970) 47.
20. R. W. DAVIDGE and J. R. PERRY, *Ceramurgica*, **3** (1973) 22.
21. A. G. EVANS and R. W. DAVIDGE, *Phil. Mag.* **20** (1969) 373.

Received 4 June and accepted 12 June 1973.